

**A Re-Analysis of The Cotton Valley Hydraulic Fracture Imaging Project:  
Imaged Geometry of the Taylor Sand Hydraulic Fractures**

**Prepared by the GRI Diagnostic Project Team**

**Sandia National Laboratories: GRI Contract No. 5096-211-2059**

**Branagan & Associates: GRI Contract No. 5097-210-3958**

**December 18, 1997**

# **A Re-Analysis of The Cotton Valley Hydraulic Fracture Imaging Project: Imaged Geometry of the Taylor Sand Hydraulic Fractures**

## **GRI Diagnostic Project Team**

### **Objectives**

The objective of this re-analysis was to examine the microseismic data from the Taylor sand hydraulic fracture injections<sup>1</sup> using a different methodology than that provided by ARCO.<sup>2</sup> The ARCO approach typically uses two-well data so that only arrival time information are needed to locate microseismic origins. In the Taylor sand injections (perforated interval: 9620-9640), data were obtained in only one well (CGU-22-09). To locate the points, ARCO assumed a fracture azimuth and located microseisms near that azimuth line. This is a reasonable approach, given the good azimuth information from the two higher injections where two-well data were available, but there is a small possibility that some unusual behavior might have occurred which would not be observed if the azimuth were assumed.

This re-analysis uses a single-well approach where p-wave particle motion is used to determine the azimuthal direction to the microseismic origin and p-wave and s-wave arrivals are used to determine the distance and the elevation of the microseism. The drawback of this method is that high quality p-waves must be obtained to get good azimuthal information. As a result, this approach cannot “see” as far as the ARCO approach, but should at least confirm the behavior on the near wing.

It was originally intended that data be extracted to produce an equivalent 5-level system (e.g., analogous to that used in the GRI M-Site project) that would mimic the measured response if a 5-level wireline array were employed in a single well. As will be seen, the data quality (at least in the Taylor sand) are not sufficient to allow a suitable 5-level system to be extracted, and all usable levels were ultimately examined to provide an adequate analysis.

### **Single-Well Approach**

The single-well approach uses data from a single vertical array of tri-axial receivers to locate microseisms. It requires that relatively clear p waves be detected, as the particle motion of the p-waves is used to determine the azimuthal direction to the microseism. Thus, the assumption is that the particle motion is in the direction of travel of the wave and it points directly back to the source, irrespective of any layering or heterogeneities. The distance to the microseism and its elevation are calculated using a joint p-wave and s-wave regression of the distance equations, assuming constant p-wave and s-wave velocities throughout the medium. However, a more detailed layered analysis can also be performed if the data are of sufficiently high quality that advanced analyses would provide more accurate results.

To perform the analysis, it is necessary that the receivers be oriented and that both x and y (the two horizontal) geophones be functioning and amplitude-balanced on numerous levels. Hodograms of the p-wave particle motion over 1-2 cycles are performed to extract the azimuth at

each level. Numerous levels must be used because individual hodograms may be in error by several degrees and some statistics are required to improve confidence levels. In this case, orientation of the receivers was performed using a RA tag and a Rotoscan log. Additionally, the crosswell survey data are also useful for verifying the Rotoscan data and the functionality of the receivers.

To extract accurate distance and elevation data, a reasonable estimate of the velocity must be made. Velocities were obtained from both sonic logs and from the crosswell survey.

### Receiver Orientation

It is assumed that the Rotoscan survey provides an accurate receiver orientation, but a check using crosswell data is always a good idea because it turns up problems that might not be otherwise noticed. To perform these checks, three primacord shots performed on April 7, 1997 were analyzed for orientation. These particular three were chosen because they were located at the bottom, top, and middle of the receiver vertical span. Files analyzed included “upr02\_2\_9515.segy” located at 9515 ft, “upr03\_2\_7856.segy”, located at 7856 ft, and “upr04\_2\_8400.segy”, located at 8400 ft. The orientations of these shots, relative to the Rotoscan, are shown in Figure 1. In general, the agreement is good, particularly in the center of the array. Several of the upper levels show considerable discrepancy, but this may be due to the distance to most of the shots. The most important feature of this plot is the large disagreement seen on four of the levels, which suggests that these levels may have been cross wired. These levels are at 7619 ft (level 7), 8069 ft (level 16), 8215 ft (level 19) and 8521 ft (level 25). The cross wiring is also suspected from examination of the microseismic data for changes in phase relationships from level to level. Tabular results from these tests are shown in Table 1. Missing data are indicative of broken channels or of shots that are too far from the receiver to be adequately analyzed. Standard deviations of 5° or less are usually indicative of a good orientation result. Many of these levels show greater standard deviations, but these could probably be improved by analyzing more of the primacord shots.

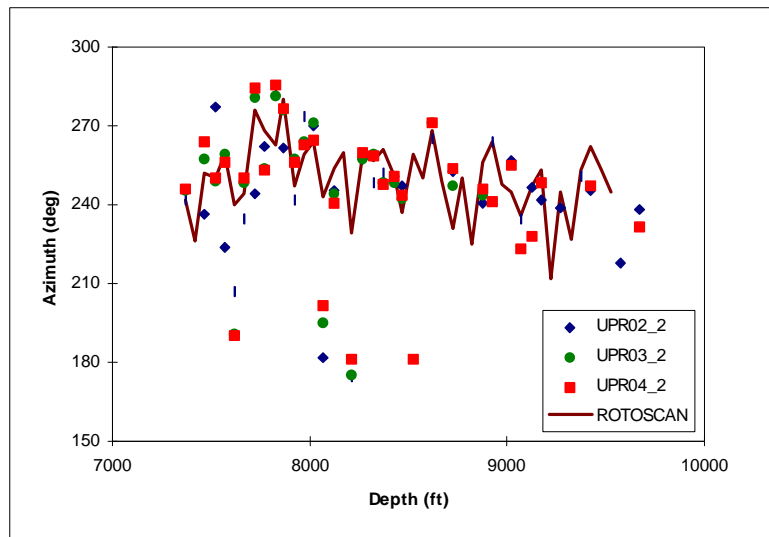


Figure 1. Comparison of primacord hodograms and Rotoscan orientations.

Table 1 Hodogram results for three primacord shots

Depth	upr02-2 azimuth	upr03-2 azimuth	upr04-2 azimuth	AVG	STD
7318					
7368	241.77	245.24	245.75	244.2533	2.165695
7418					
7468	236.62	257.38	263.74	252.58	14.18286
7519	277.23	249.18	249.97	258.7933	15.97151
7569	223.61	259.04	256.32	246.3233	19.71728
7619	206.81	190.91	190.38	196.0333	9.336629
7669	234.75	248.44	250.04	244.41	8.403969
7719	244.05	280.98	284.22	269.75	22.31573
7769	262.41	253.85	253.29	256.5167	5.111451
7823	281.86	281.36	285.9	283.04	2.489418
7870	261.69	275.99	276.89	271.5233	8.527798
7920	241.85	257.58	256.44	251.9567	8.771171
7970	273.77	264.07	262.66	266.8333	6.048556
8019	270.18	270.98	264.64	268.6	3.452709
8069	181.79	195.29	201.36	192.8133	10.01732
8119	245.56	244.36	240.3	243.4067	2.756544
8171					
8215	174.85	175.23	181.03	177.0367	3.463543
8271	257.46	257.7	259.8	258.32	1.287323
8321	248.52	259.17	258.43	255.3733	5.946683
8371	251.97	248.66	248.08	249.57	2.098595
8431	250.92	248.47	250.54	249.9767	1.318572
8471	247.21	242.39	243.4	244.3333	2.541935
8521			181.24	181.24	
8571					
8621	265.43	270.95	271.34	269.24	3.305314
8671					
8722	252.64	247.5	253.95	251.3633	3.409257
8773					
8823					
8873	240.78	243.7	245.9	243.46	2.568424
8923	264.01		241.01	252.51	16.26346
8973					
9023	256.91		255	255.955	1.350574
9073	234.82		223.27	229.045	8.167083
9123	246.74		227.86	237.3	13.35018
9173	241.73		248.5	245.115	4.787113
9223					
9274	238.79			238.79	
9324					
9374	250.86			250.86	
9425	245.17		247.18	246.175	1.421285
9475					
9525					
9575	217.73			217.73	
9625					
9675	238.42		231.49	234.955	4.90025

## Velocity Structure

Accurate microseism location relies on accurate knowledge of the formation velocities. For this test, velocities were obtained from both a dipole sonic log and a crosswell survey produced by John Fairborn from the primacord and vibrator shots.<sup>3</sup> Table 2 lists estimated sonic-log velocities taken over limited intervals. Given that the microseismic analyses require average velocities, these data yield an average p-wave velocity of 14,500 ft/sec and an average s-wave velocity of 8,400 ft/sec.

Table 2 Estimated interval velocities from sonic log

Depths (ft)	Compressional Velocity (ft/sec)	Shear Velocity (ft/sec)
9265-9330	15,400	10,000
9330-9365	13,300	7,700
9365-9400	14,300	8,500
9400-9512	13,300	7,400
9512-9540	16,700	9,100
9540-9570	14,300	8,000
9570-9660	15,400	9,100
9660->	13,300	7,100

Generally, a crosswell survey yields better velocity estimates because it is conducted at frequencies more representative of the microseisms and it samples a larger section of the formation. Based upon the crosswell results, the average p-wave velocity is 15,100 ft/sec and the average s-wave velocity is 9,000 ft/sec. The velocities from the crosswell survey are approximately 600 ft/sec faster than that obtained from the log.

## Receiver Characteristics

Upon examination of crosswell primacord shots and subsequent microseismic data, it was found that a number of the receiver levels had some problems that limited their usefulness. Table 3 shows a listing of the levels, their depths, the Rotoscan azimuths, the observed problems, and levels at which hodograms could be accurately made. Of particular interest for the Taylor sand operations is the bottom of the array, as these receivers are closest to the microseisms and the energy will travel through the fewest layers to reach the receivers. Unfortunately, the bottom of the array has very few levels which are responding adequately. There is only one level in the vicinity of the Taylor sand on which good hodograms can be obtained. The next closest level is 350 ft above, and the next hodogram level is an additional 200 ft above. In general, the best hodogram data are obtained from p-waves which are traveling within the horizontal layers. As a result, the hodogram information for this test will have a relatively large uncertainty.

Table 3 Receiver level characteristics

LEVEL	DEPTH	ROTOSCAN	PROBLEMS	HODOGRAMS
1	7318	148	NO X	
2	7368	242	NOZ	HODOGRAM
3	7418	226	NO X,Z	
4	7468	252		HODOGRAM
5	7519	250		HODOGRAM
6	7569	259		HODOGRAM
7	7619	240	POOR X,Y	
8	7669	244		HODOGRAM
9	7719	276		HODOGRAM
10	7769	268	BROKE	
11	7823	263		HODOGRAM
12	7870	280		HODOGRAM
13	7920	247	BROKE	
14	7970	259	BROKE	
15	8019	264	NO X	
16	8069	243	CROSS WIRED	
17	8119	254	NO Z	HODOGRAM
18	8171	260	NO X,Z	
19	8215	229	CROSS WIRED	
20	8271	259		HODOGRAM
21	8321	257		HODOGRAM
22	8371	261		HODOGRAM
23	8431	251		HODOGRAM
24	8471	237		HODOGRAM
25	8521	259	BROKE	
26	8571	250	BROKE	
27	8621	268	BROKE	
28	8671	249	BROKE	
29	8722	231	BROKE	
30	8773	250	NO Z	HODOGRAM
31	8823	225	BROKE	
32	8873	256	BROKE	
33	8923	264		HODOGRAM
34	8973	248	NO Z	HODOGRAM
35	9023	245	NO Y	
36	9073	236	NO X,Y	
37	9123	247	BROKE	
38	9173	253		HODOGRAM
39	9223	212	BROKE	
40	9274	245	BROKE	
41	9324	227	BROKE	
42	9374	253	BROKE	
43	9425	262	NO X,Z	
44	9475	253	BROKE	
45	9525	245	NO Z	HODOGRAM
46	9575		POOR X,Y	
47	9625		BROKE	
48	9675		NO X	

## Microseism Characteristics

The general characteristics of the microseisms were that they had large, easily visible s waves on most levels (although they were often obscured on the lowest levels), but easily visible p waves only on the lower levels. Typically, p waves that were observable on the upper levels had considerable scatter in their hodogram azimuths and consequently were seldom used.

The spectral content of most of the microseisms were relatively broad band, as seen in both the p-wave example in Figure 2 and the s-wave example in Figure 3. This behavior suggests that there were no internal resonances with the receiver or transducer (as would be expected since they were grouted in place), but also suggests that there may be considerable energy at higher frequencies which could not be captured with the 1 msec sampling rate. As can be seen from the amplitude relationships, the receivers were generally oriented with the y axis pointing toward the microseisms. There are large amplitudes on the y axis of the p wave and the large amplitudes on the x axis of the s wave.

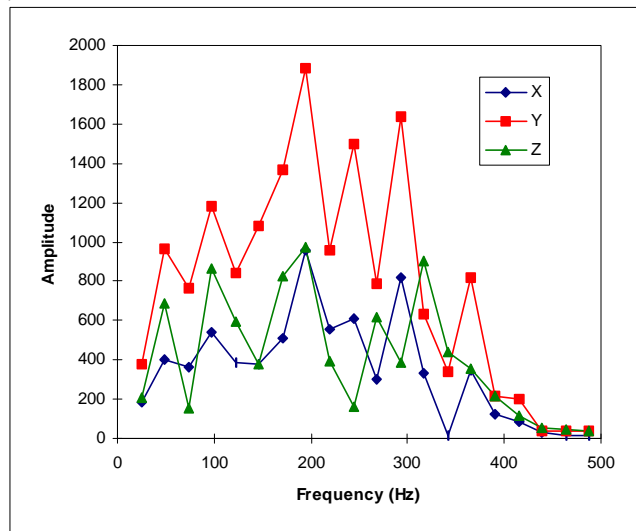


Figure 2. Spectrum of p wave for file 970512132341.04597.segy

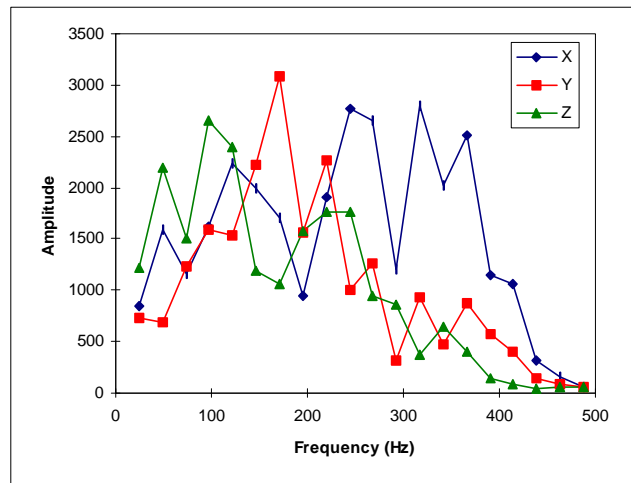


Figure 3. Spectrum of s wave for file 970512132341.04597.segy

Table 4 shows an example data set taken from one of the microseisms. This suite of data, which starts at level 16 (few p-waves could be observed above 8000 ft), is relatively sparse, particularly at the 9600 ft interval (the frac interval). Only eight usable hodograms have been extracted, with considerable scatter in the absolute azimuth. The hodogram azimuth on level 46 is referenced to the crosswell orientations, as there was no Rotoscan data for the bottom three levels. Thus, the discrepancy in absolute angle between it and higher levels may be due to orientation errors. Note also that there are fewer hodograms in Table 4 than possible (e.g., Table 3) because some levels may not provide sufficiently clear p waves to produce good quality hodograms.

Table 4. Example microseism data set

Depth	Orientation	Level	Azimuth	Inclination	P-Arrival	S-Arrival	Abs Azimuth
8069	243	16			450	526	
8119	254	17				521	
8171	260	18				519	
8215	229	19				513	
8271	259	20	-28.58	24.64	433	510	50.42
8321	257	21					
8371	261	22	-19.8	25.68	424	501	61.2
8431	251	23	-22.16	47.08	429	495	48.84
8471	237	24	-9.37	18.79	427	494	47.63
8521	259	25					
8571	250	26					
8621	268	27					
8671	249	28					
8722	231	29					
8773	250	30					
8823	225	31					
8873	256	32					
8923	264	33	-45.88	25.36	403	462	38.12
8973	248	34	-17.55	11.19	401	461	50.45
9023	245	35			401	461	
9073	236	36			399	461	
9123	247	37					
9173	253	38	-24.5	27.14	396	454	48.5
9223	212	39					
9274	245	40					
9324	227	41					
9374	253	42					
9425	262	43					
9475	253	44					
9525	245	45					
9575	218	46	-3.53	0.03	388	447	34.47
9625	226	47					
9675	235	48			390	452	

## Results

Sixty eight microseisms were found to be locatable using the single-well approach. Minimum requirements for analysis were two hodogram azimuths and at least one p-wave arrival (if there were also several s-wave arrivals) or at least one s-wave arrival (if there were also several p-wave arrivals). Using the velocities derived from the averaging of the crosswell survey, Figures 4 and 5 show plan view and side view maps of the analyzed microseisms. These data are very similar to the ARCO results, yielding a long, well-contained fracture whose azimuth is N80°E. However, there are some differences in the scatter and the lack of intersection of the microseisms with the fracture well. Even more significant differences arise when one considers the effect of the velocity uncertainty.

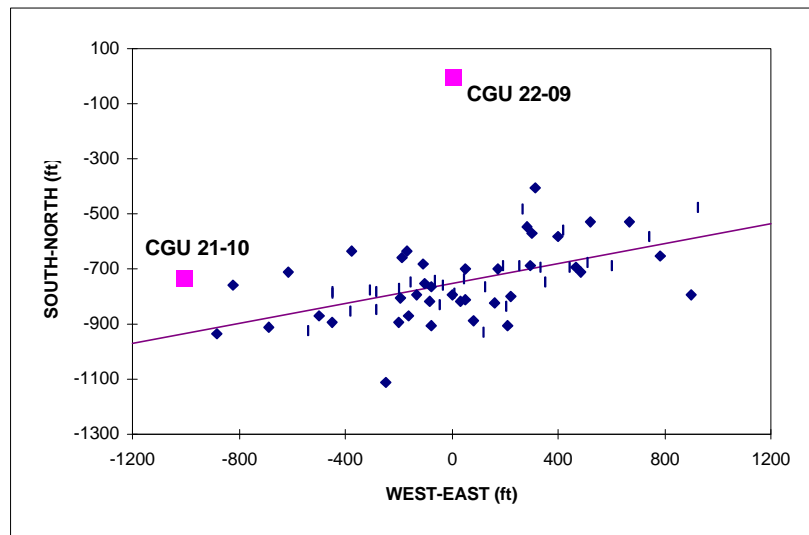


Figure 4. Plan view of Taylor sand fracture map for all three stages.

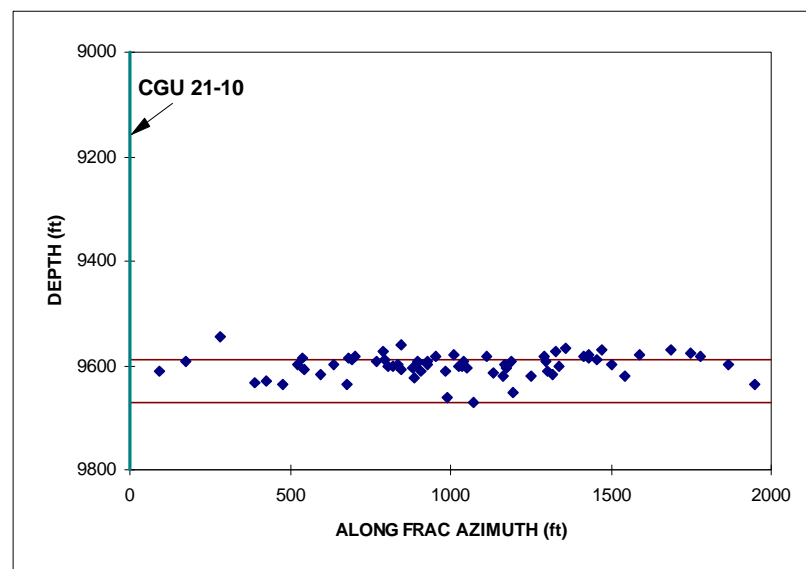


Figure 5. Side view of Taylor sand fracture map for all three stages.

Because of the array configuration (no receivers below the frac interval and few usable receivers across from the frac interval), small changes in velocity result in significant changes in the map. For example, Figures 6 and 7 show the maps that would result if the log-derived velocities were used. In this case, the plan view map appears to more closely intercept the fracture well, but all of the microseisms are now located about 100 ft above the Taylor sand.

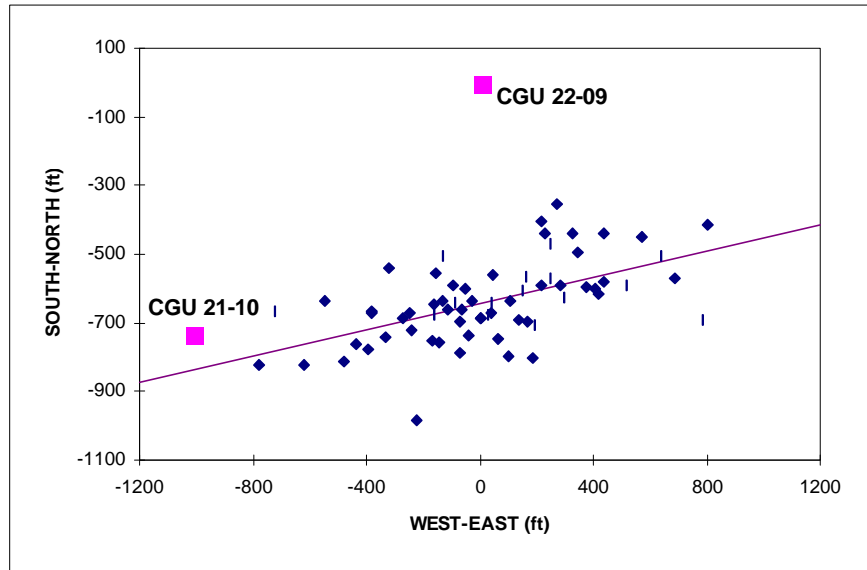


Figure 6. Revised plan view map using log-derived velocities.

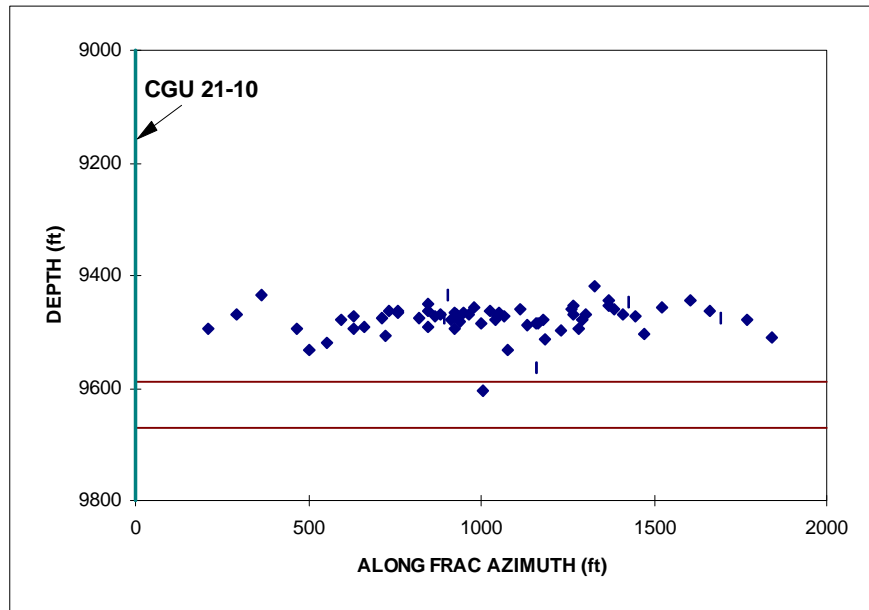


Figure 7. Revised side view map using log-derived velocities.

If velocities more typical of ARCO's ( $p=16,500$  ft/sec;  $s=10,000$  ft/sec; without anisotropy) are used, then the points locate approximately 100 ft below the Taylor sand. As ARCO has shown, anisotropic velocities can remedy the problem and bring the points back into the sand and have the plan view image intersect the fracture well.

At this time, it is believed that the data in Figures 4 and 5 represent the best image of this data set that can be obtained from the single-well approach. A listing of the data points are shown in Tables 5 and 6 for stages 1-2 and 3, respectively. The east and north locations are relative to the monitor well, the "result" is the projection of the location on the azimuth regression line, and the depth is relative to the monitor well. The last three columns are more interesting, as they provide uncertainty data taken from the joint  $p$ - $s$  regression and the hodogram statistics. Generally, the height uncertainty is small because of the large number of receivers in the vertical plane, but this uncertainty assumes that the velocity structure is correct. Velocity uncertainties have a further effect on the uncertainty. The distance uncertainty is also relatively small because of the large number of receivers, with the same caveats relative to the velocity structure. The largest error is associated with the azimuth, primarily because there are so few receivers laterally adjacent to the fracture interval. Angular uncertainties of  $10^\circ$  at 1000 ft result in lateral uncertainties of 173 ft and angular uncertainties of  $20^\circ$  at 1000 ft work out to 340 ft. These uncertainties are not large enough to affect the overall results, but they do demonstrate how important it is (1) to have high quality receivers and data acquisition and (2) to have the array strategically placed.

Table 5. Listing of Taylor sand microseismic locations and uncertainty data - Stage 1 & 2

east	north	result	depth	Height sd	Dist sd	Angle sd
-448.88	-892.28	521.31	9598.32	8.41	47.57	12.53
-500.17	-871.00	474.66	9634.88	6.67	29.43	7.31
-687.39	-911.90	283.15	9546.19	16.07	37.21	11.65
-542.74	-924.66	423.17	9629.40	14.45	30.77	7.75
-824.24	-757.14	176.27	9592.98	12.10	53.76	8.15
-879.72	-932.62	90.22	9611.43	9.65	41.21	9.14
-161.94	-871.51	807.32	9600.65	10.90	59.03	15.74
-285.15	-779.65	702.58	9582.89	6.90	41.84	10.20
-79.31	-905.17	882.57	9604.61	9.63	54.46	13.28
-383.09	-854.46	592.81	9617.78	7.92	46.63	12.12
-195.53	-768.90	792.68	9588.63	5.23	36.20	11.72
-191.03	-806.17	790.42	9573.67	7.29	38.25	13.82
-134.05	-796.77	848.16	9606.37	6.12	38.74	10.00
-80.03	-817.51	897.58	9593.21	10.58	67.96	11.48
-152.75	-749.03	838.33	9597.53	10.77	72.46	20.59
-106.85	-682.66	895.39	9594.37	7.20	50.08	15.74
-77.53	-764.56	909.55	9609.57	5.37	38.51	12.62
5.13	-794.57	985.48	9610.45	5.12	33.07	8.04
-9.84	-737.57	979.57	9598.29	4.42	25.86	15.44
-32.85	-757.05	954.84	9583.25	11.25	63.38	12.08
-281.46	-848.05	693.94	9590.10	8.00	44.47	10.19
-165.34	-633.74	846.61	9559.89	8.17	59.38	21.60
-44.69	-830.43	930.04	9593.20	6.75	38.37	6.25
174.51	-702.37	1168.65	9598.71	5.20	28.96	5.79
127.32	-766.51	1110.73	9581.58	6.44	42.31	12.41
-100.51	-751.30	889.31	9625.02	4.60	32.52	4.77
116.08	-931.33	1070.11	9670.12	16.26	108.27	7.11
254.37	-687.66	1249.85	9621.63	5.86	32.50	8.67
45.13	-738.19	1034.94	9602.54	5.58	34.35	16.35
162.28	-823.57	1134.88	9613.16	6.94	32.18	13.58
-63.32	-738.98	928.11	9599.52	3.54	23.98	9.78

Table 6. Listing of Taylor sand microseismic locations and uncertainty data - Stage 3

east	north	result	depth	Height sd	Dist sd	Angle sd
-196.80	-893.10	769.15	9590.70	6.28	22.83	18.29
53.99	-699.66	1050.57	9605.35	3.33	23.88	9.41
208.89	-905.02	1166.12	9621.69	23.97	52.52	4.94
-186.07	-660.40	821.44	9602.44	15.35	102.69	11.46
49.43	-813.27	1025.71	9601.63	4.49	26.44	14.57
193.93	-688.15	1190.31	9592.74	5.92	26.86	17.25
-446.39	-783.40	543.28	9606.73	5.94	26.24	9.18
282.75	-549.00	1302.64	9609.93	7.30	45.88	9.29
-447.52	-790.76	540.85	9585.71	6.66	35.85	8.56
402.55	-581.70	1414.63	9582.51	5.50	36.79	12.23
6.56	-788.03	988.06	9660.69	9.93	19.14	5.60
353.44	-745.93	1336.87	9602.44	4.30	23.53	13.51
79.91	-887.68	1042.35	9591.26	6.73	34.20	12.11
220.09	-801.64	1195.69	9652.79	6.29	24.08	15.22
312.46	-406.40	1357.45	9567.15	10.68	81.88	10.43
-615.38	-711.69	389.89	9633.06	8.28	35.21	18.88
466.56	-695.26	1457.24	9588.52	4.31	26.17	11.36
33.15	-816.91	1009.04	9580.89	4.07	23.74	4.14
598.64	-685.89	1588.86	9580.15	3.60	18.31	12.35
-308.13	-777.19	680.42	9585.60	3.37	23.43	8.21
334.27	-696.83	1326.81	9573.64	5.82	26.54	14.97
-249.79	-1113.73	677.46	9636.72	10.18	35.24	7.01
415.38	-557.60	1431.58	9580.29	3.37	21.62	7.51
440.69	-696.56	1431.56	9585.45	3.65	20.48	9.92
669.27	-526.91	1686.86	9568.76	5.85	33.34	4.93
785.55	-653.84	1778.48	9583.84	6.47	20.89	9.24
203.74	-836.86	1173.29	9603.59	12.70	58.33	10.89
304.02	-571.10	1319.61	9618.43	7.00	43.82	20.81
509.88	-677.15	1503.10	9599.41	6.35	31.27	12.72
487.22	-713.95	1474.21	9569.28	8.74	47.34	6.48
740.44	-582.22	1746.95	9576.96	7.94	31.12	18.78
262.88	-481.69	1295.17	9592.41	3.84	32.02	7.57
524.87	-528.74	1544.47	9619.74	5.32	27.18	13.58
927.99	-476.96	1950.34	9636.78	5.37	24.43	7.41
901.48	-794.95	1867.23	9599.03	7.73	32.59	13.33
298.27	-685.81	1293.37	9584.16	3.66	22.23	1.88

## Discussion

We find that there is no unique solution to calculating the microseismic locations for this array geometry (single well, all receivers above the interval, sparse data set) because of the uncertainty in the velocity structure and the sparse array at the fracture depth. The two later fracture experiments, with receivers in two wells and both above and below the fracture interval, provide much more constraint and limit most uncertainty due to velocity structure.

A major issue associated with these maps is the lack of any microseisms on the far wing of the fracture. Given that this single-well analysis requires a number of clear p waves for accurate location, it is not believed that any microseisms of the magnitudes seen here could have been observed at distances greater than the wellbore location (about 1200-1300 ft horizontally). Other analyses - such as ARCO's - which do not need polarization information can extract locations from greater distances, and may be able to observe microseisms of the strengths found here at distances representative of the far wing. Such is not true for these single-well approaches. The subsequent Imaging Project fracture experiments, however, have much larger amplitude microseisms and it may be possible to detect them from as far away as the opposite wing using this approach.

Since (1) the microseismic data have relatively low-level amplitudes, (2) the receivers are poorly distributed relative to the fracture's vertical location, and (3) there is considerable uncertainty in the velocity structure, advanced analyses of the microseismic locations using a layered medium do not appear warranted. Such an analysis would account for the layering and its effect on the ray paths.

Although it was originally intended to to extract 5-level data from this data set for comparison calculations, the quality of the data and the limited receivers at the depth of the fracture make this a futile exercise. However, the uppermost fracture interval is suitably placed relative to the working receivers to make that test a good comparison case. This analysis will be done at a later time.

## Conclusions

- This re-analysis of the Taylor sand microseismic data shows general agreement with the ARCO analysis using a different analysis approach.
- The fracture appears to be about 2000 ft long on the east wing with a well-contained height and an azimuth of N80°E. However, some uncertainties remain because of the limited velocity structure information and the skewed receiver array.
- Using this approach, it appears that no microseisms could be observed on the far wing of the fracture unless they were much stronger than those generally observed in this test.
- No further analyses of the Taylor sand data appears reasonable at this time.
- Additional analyses of the upper fracture will be performed at a later time.

## References

1. Walker, R.N., "Cotton Valley Hydraulic Fracture Imaging Project", SPE38577, Proceedings, SPE Annual Technical Conference and Exhibition, San Antonio, TX, October 5-8, 1997.
2. Withers, R.J. and Dart, R.P., "Cotton Valley Production Stimulation Hydrofracture Microseismic Monitoring and Imaging," Data Collection & Analysis Report, ARCO Exploration & Production Technology, June 1997.
3. Fairborn, J., "Crosswell Seismic Survey, Carthage Gas Field, CGU 21-10 - CGU21-09 and CGU21-10 - CGU 22-09," Paulsson Geophysical Services Inc. Report, June 12, 1997.